Spatial properties of integrable and nonintegrable discrete nonlinear Schrödinger equations

D. Hennig,[1,2] N. G. Sun,[1,2] H. Gabriel,[1] and G. P. Tsironis[2,3]
[1]*Freie Universität Berlin, Fachbereich Physik, Institut für Theoretische Physik, Arnimallee 14, 14195 Berlin, Germany*
[2]*Center for Nonlinear Science, and Department of Physics, University of North Texas, Denton, Texas 76203*
[3]*Physics Department, University of Crete and Research Center of Crete, P.O. Box 1527, Heraklion 71110, Crete, Greece*
(Received 21 December 1994)

We study the spatial properties of a nonlinear discrete Schrödinger equation introduced by Cai, Bishop, and Grønbech-Jensen [Phys. Rev. Lett. **72**, 591 (1994)] that interpolates between the integrable Ablowitz-Ladik equation and the nonintegrable discrete nonlinear Schrödinger equation. We focus on the stationary properties of the interpolating equation and analyze the interplay between integrability and nonintegrability by transforming the problem into a dynamical system and investigating its Hamiltonian structure. We find explicit parameter regimes where the corresponding dynamical system has regular trajectories leading to propagating wave solutions. Using the anti-integrable limit, we show the existence of breathers. We also investigate the wave transmission problem through a finite segment of the nonlinear lattice and analyze the regimes of regular wave transmission. By analogy of the nonlinear lattice problem with chaotic scattering systems, we find the chain lengths at which reliable information transmission via amplitude modulation is possible.

PACS number(s): 05.45.+b, 42.65.Pc, 71.10.+x, 78.20.Dj

I. INTRODUCTION

The nonlinear Schrödinger (NLS) equation is one of the prototypical nonlinear partial differential equations, the study of which has led to fundamental advances in nonlinear dynamics. The study of the NLS equation was motivated by a large number of physical and mathematical problems ranging from optical pulse propagation in nonlinear fibers to hydrodynamics, condensed matter physics, and biophysics. We now know that the NLS equation provides one of the few examples of completely integrable nonlinear partial differential equations [1]. Since most work in nonlinear wave propagation involves at some stage a numerical study of the problem, the issue of the discretization of the NLS equation was addressed early in Ref. [1]. Ablowitz and Ladik notices that among a large number of possible discretizations of the NLS equation there is one that is also integrable [2]. The study of the integrable version of the discrete nonlinear Schrödinger equation, called hereafter the Ablowitz-Ladik, or AL equation, showed that it has solutions which are essentially the discrete versions of the NLS solitons [2]. Another discrete version of the NLS equation was studied in detail later [3]; the latter, usually referred to as the discrete nonlinear Schrödinger (DNLS) equation or the discrete self-trapping (DST) equation, has quite a number of interesting properties, but it is not integrable [4]. We note that the motivation for studying the two discrete versions of the NLS equation, viz., the AL equation and the DNLS equation, respectively, are quite different: The AL equation, on one hand, has very interesting mathematical properties, but not very clear physical significance; the introduction of the DNLS equation, on the other hand, is primarily motivated physically. In particular, the latter seems to arise naturally in the context of energy localization in discrete condensed matter and biological systems as well as in optical devices [3–9]. Even though in these problems one typically assumes that the length scale of the nonlinear wave is much larger than the lattice spacing and therefore the NLS equation provides a good description for those problems, the study of the DNLS (and AL) equation is important when the size of the physical system is small or the nonlinear wave is strongly localized. In such cases, the interplay between nonlinearity and discreteness can lead to novel effects, not present in the continuum analysis. In particular, novel properties such as the possible absence of localization in the DNLS or AL system in the presence of disorder can occur [10–12].

The motivation for the present paper is an equation introduced recently by Cai, Bishop, and Grønbech-Jensen [13] that interpolates between DNLS and AL equations while containing these two as its limits [14]. By varying the two nonlinearity parameters of this new equation one is able to monitor how "close" it is to the integrable or nonintegrable version of the NLS equation. The new equation finds its physical explanation in the context of the nonlinear coupler problem [16]. However, its basic merit is that it allows us to study the interplay of the integrable and nonintegrable NLS-type terms in discrete lattices. In addition, one can address the issue of "nonlinear eigenstates" of the new equation and their connection to the integrability-nonintegrability issue.

The present paper is organized as follows. In Sec. II we introduce the model with the combined integrable and nonintegrable discrete-nonlinear-Schrödinger-equation-type terms and investigate its stationary solutions and their stability. We apply converse Kolmogorov-Arnold-Moser (KAM) theory to identify stability regions and use the concept of the anti-integrable limit to show the existence of breathers. In Sec. III we use the conservation of probability current to turn the nonlinear lattice equa-

tions into a two-dimensional real map, and investigate the stability properties and bifurcation behavior of the map dynamics. We place particular emphasis on the route to chaos via a period-doubling sequence. In Sec. IV we investigate the wave transmissivity from a Hamiltonian scattering point of view and show numerical results for the transmitted intensity of the "fixed output" problem. We summarize our results in Sec. V.

II. DESCRIPTION OF THE MODEL FOR THE NONLINEAR DISCRETE SCHRÖDINGER EQUATION

The main purpose of this paper is to study the following stationary discrete nonlinear Schrödinger equation:

$$E\phi_n-(1+\mu|\phi_n|^2)[\phi_{n+1}+\phi_{n-1}]+\gamma|\phi_n|^2\phi_n=0\ , \tag{1}$$

where ϕ_n is a complex amplitude, μ and γ are nonlinearity parameters, and E is the phase of the stationary ansatz. Equation (1) is obtained from the following time-dependent nonlinear discrete Schrödinger equation:

$$i\frac{d\psi_n(t)}{dt}=[1+\mu|\psi_n(t)|^2][\psi_{n+1}(t)+\psi_{n-1}(t)] -\gamma|\psi_n(t)|^2\psi_n(t)\ , \tag{2}$$

by substituting $\psi_n(t)=\phi_n\exp(-iEt)$ in Eq. (2). We note that Eq. (2) interpolates between two well studied discretizations of the NLS equation, viz., the DNLS and AL equations obtained by setting $\mu=0$ (with $\gamma\neq0$) and $\gamma=0$ (with $\mu\neq0$), respectively [13]. The time-dependent properties of Eq. (2) were partly discussed in Refs. [13,15] whereas its stationary properties in the aforementioned extreme limits were analyzed through map approaches in Refs. [17–20]. The stationary real-valued AL system satisfies an integrable mapping which is contained in the 18-parameter family of integrable mappings of the plane reported by Quispel, Roberts, and Thompson in [21]. In this paper we will present an analysis of Eq. (1) and discuss the interplay of the integrable and nonintegrable nonlinear terms in the context of the complete equation.

Equation (1) may be rewritten as

$$\phi_{n+1}+\phi_{n-1}=\frac{E+\gamma|\phi_n|^2}{1+\mu|\phi_n|^2}\phi_n\ , \tag{3}$$

which obviously reduces to a degenerate linear map if $\gamma=E\mu$. Although reduction of the complex-valued amplitude dynamics to a two-dimensional real-valued map is possible (see Sec. III), we concentrate in this section on the study of the recurrence relation $\phi_{n+1}=\phi_{n+1}(\phi_n,\phi_{n-1})$ appropriate for the investigation of stability of the nonlinear lattice chain. Equation (3) can also be derived as the relation which makes the action functional

$$F=\sum_n\left\{\frac{1}{\mu}\left[E-\frac{\gamma}{\mu}\right]\ln(1+\mu|\phi_n|^2)+\frac{\gamma}{\mu}|\phi_n|^2 -(\phi_n^*\phi_{n+1}+\phi_n\phi_{n+1}^*)\right\} \tag{4}$$

an extremum. In the limit $\mu=0$, the latter is replaced by

$$F=\sum_n\{E|\phi_n|^2+\tfrac{1}{2}\gamma|\phi_n|^4-(\phi_n^*\phi_{n+1}+\phi_n\phi_{n+1}^*)\}\ . \tag{5}$$

The extremal sets $\{\phi_n\}$ define the orbits and together with appropriate boundary conditions determine the solutions of a particular physical problem. However, concerning the stability properties one has to distinguish between the (dynamical) stability of the physical solutions and the (linear mapping) stability of the corresponding map orbit generated by the recurrence relation $\phi_{n+1}=\phi_{n+1}(\phi_n,\phi_{n-1})$ [22,23]. In general, a dynamical stable (metastable in Aubry's terminology) solution minimizing the action corresponds to a linearly unstable map orbit, whereas physically unstable solutions corresponding to maximum energy configurations are reflected in the map dynamics as linearly stable orbits. In the present study we focus on the transmission properties of the "nonlinear lattice" of Eq. (1), since finding the linearly stable map solutions (propagating wave solutions) is essential.

A. Stability and regular solutions

The second-order difference equation (3) can be regarded as a symplectic nonlinear transformation relating the amplitudes in adjacent lattice sites. This transformation can be considered as a dynamical system where the lattice index n plays the role of the discrete time n. The resulting dynamics of the two-component (amplitude) vector $(\phi_{n+1},\phi_n)^T$ is determined by the following Poincaré map:

$$\mathcal{M}_n:\ \begin{bmatrix}\phi_{n+1}\\ \phi_n\end{bmatrix}=\begin{bmatrix}E_n & -1\\ 1 & 0\end{bmatrix}\begin{bmatrix}\phi_n\\ \phi_{n-1}\end{bmatrix}\ , \tag{6}$$

where the nonlinear transfer matrix depends on the amplitude ϕ_n through

$$E_n=\frac{E+\gamma|\phi_n|^2}{1+\mu|\phi_n|^2}\ . \tag{7}$$

The stability of the orbits $\{\phi_n\}$, $(n=0,\ldots,N)$, or equivalently the transmission properties of the nonlinear lattice of chain length N, is governed by the solution behavior of the corresponding linearized equations in the neighborhood of an orbit ranging from (ϕ_0,ϕ_1) to (ϕ_{N-1},ϕ_N). For a semi-infinite (or infinite) one-dimensional lattice chain the (finite) sequence $\{\phi_n\}$ $(n=0,\ldots,N)$ defines an orbit segment. Mapping the variations from $(\delta\phi_0,\delta\phi_1)$ to $(\delta\phi_{N-1},\delta\phi_N)$ is accomplished by the product of the real 2×2 symplectic Jacobian transfer matrices

$$J(\mathcal{M})=\prod_{n=1}^{N-1}J(\mathcal{M}_n)\ , \tag{8}$$

where $J(\mathcal{M}_n)=[\partial(\phi_{n+1},\phi_n)]/\partial(\phi_n,\phi_{n-1})]$ is the real unimodular matrix

$$J(\mathcal{M}_n)=\begin{bmatrix}\tilde{E}_n(|\phi_n|) & -1\\ 1 & 0\end{bmatrix}\ , \tag{9}$$

with

$$\tilde{E}_n(|\phi_n|)=\frac{[E+2\gamma|\phi_n|^2+\mu\gamma|\phi_n|^4]}{[1+\mu|\phi_n|^2]^2} . \tag{10}$$

Before proceeding with the stability analysis of the nonlinear discrete Schrödinger equation (1), we note that in the corresponding linear tight-binding model given by the equation $\phi_{n+1}+\phi_{n-1}=E\phi_n$, the (stable) solutions in the passing band of $|E|<2$ are parametrized by a wave vector $k\in[-\pi,\pi]$ corresponding to the linear dispersion relation $E=2\cos(k)$. Upon increasing the nonlinearity parameters γ and μ from zero, the nonlinear dispersion relation for $\phi_n=\phi_0=\text{const}$ reads as $E=2\cos(k)+[2\mu\cos(k)-\gamma]|\phi_0|^2$ and the stability of the orbits can alter where rational values of the winding number $k/(2\pi)=p/q$, with integers p,q, yield periodic orbits whereas irrational values result in quasiperiodic orbits.

First, we study the linear stability of periodic orbits $\phi_{n+q}=\phi_n$ with cycle lengths q. The linear stability of a periodic orbit is governed by its multipliers, i.e., the eigenvalues of the corresponding linearized map. In examining the linear stability of the periodic orbits we make use of the fact that solving the linearized equations becomes equivalent to a band problem of a linear discrete Schrödinger (tight-binding) equation with periodic potential (see, e.g., [24–26]) where we can invoke the (linear) transfer matrix method [27].

In the following we derive a sufficient criterion for linear stability. We substitute $\delta\phi_n\equiv\varphi_n$, and the linearized equation corresponding to (3) can be written in matrix notation

$$\begin{bmatrix}\varphi_{n+1}\\ \varphi_n\end{bmatrix}=M_1(\tilde{E}_n)\begin{bmatrix}\varphi_n\\ \varphi_{n-1}\end{bmatrix} , \tag{11}$$

where $M_1(\tilde{E}_n)\equiv J(\mathcal{M}_n)$ and $\tilde{E}_n$ are given in Eqs. (9) and (10), respectively. The matrix product

$$M_q=\prod_{n=0}^{q-1}M_1(\tilde{E}_n) \tag{12}$$

transfers (φ_0,φ_{-1}) to $(\varphi_q,\varphi_{q-1})$ through a complete periodic cycle of length q. Since the periodic orbit members enter the individual transfer matrices $M_1(\tilde{E}_n)$, Eq. (11) represents a linear equation with periodic potential $\tilde{E}_n=\tilde{E}_n(|\phi_n|)$ and $\varphi_{n+q}=\exp(ikq)\varphi_n$ [28]. Thus M_q has eigenvalues $\exp(\pm ikq)$, and its trace is given by

$$\mathrm{Tr}[M_q]=2\cos(kq) , \tag{13}$$

which leads to the condition $|\mathrm{Tr}[M_q]|\le 2$ for the stable Bloch solutions and to two equivalence classes for the total symplectic transfer matrix M_q corresponding to different stability properties. For the real unimodular matrix M_q these equivalence classes are determined by the solution of the eigenvalue problem,

$$\alpha^2-(\mathrm{Tr}[M_q])\alpha+1=0 , \tag{14}$$

where the roots $\alpha_{1,2}$ determine the multipliers of the periodic orbit [29]. When $|\mathrm{Tr}[M_q]|<2$, then M_q has a pair of complex conjugate eigenvalues $\alpha_{1,2}$ on the unit circle leading to a stable elliptic periodic cycle or an oscillating Bloch-type solution (passing band state). When $|\mathrm{Tr}[M_q]|>2$, this yields real reciprocal eigenvalues corresponding to an unstable hyperbolic periodic cycle which has to be excluded as physically unacceptable, since it increases exponentially with larger chain length (stop band or gap state).

Computation of $\mathrm{Tr}\{\prod_{n=0}^{q-1}[M_1(\tilde{E}_n)]\}$ for a general periodic orbit of arbitrary cycle length q requires tedious algebra. However, if γ, μ, and E satisfy the inequality

$$E\mu\ge\gamma , \tag{15}$$

then $|\tilde{E}_n(|\phi_n|)|<|E|$ and each individual transfer (Jacobian) matrix M_1 has the important property

$$\|M_1(\tilde{E}_n)\|\le\|T_1(E_n)\| , \tag{16}$$

where

$$T_1(E_n)=\begin{bmatrix}E_n & -1\\ 1 & 0\end{bmatrix} \tag{17}$$

is the individual unimodular transfer matrix of a linear lattice chain at constant $E_n=E$. The norm of a matrix A is defined by $\|A\|=\max_{\|z\|=1}\|Az\|$, i.e., the natural norm induced by the vector norm $\|z\|$ [30]. We note that the inequality (16) imposes no restriction to the amplitudes ϕ_n, since it is a global feature of the mapping in the parameter range satisfying (15). For the linear lattice chain the total transfer matrix satisfies $|\mathrm{Tr}[T_q(E)]|=|\mathrm{Tr}[\prod_{n=0}^{q-1}T_1(E_n)]|<2$ as long as $|E_n|=|E|<2$, i.e., is in the range of the passing band. Furthermore, because all the local Jacobians are identical, it is easy to show that the global trace $\mathrm{Tr}[T_q(E)]=2\cos(\theta q)$, where $\theta=\cos^{-1}(\frac{1}{2}\mathrm{Tr}[T_1])=\cos^{-1}(\frac{1}{2}E)$. With the help of $\|A^n\|\le\|A\|^n$ and the modified inequality (16),

$$\prod_{n=0}^{q-1}\{\|T_1(E_n)\|-\|M_1(\tilde{E}_n)\|\}\ge 0 , \tag{18}$$

we infer that

$$\left|\left|\prod_{n=0}^{q-1}[T_1(E_n)]\right|\right|\ge\left|\left|\prod_{n=0}^{q-1}[M_1(\tilde{E}_n)]\right|\right| . \tag{19}$$

Further, a natural matrix norm satisfies the inequality

$$\max|\alpha_{1,2}|\le\|A\| . \tag{20}$$

Using (19) and (20), one sees that the spectral radius of the matrix $\prod_{n=0}^{q-1}[T_1(E_n)]$ forms a majorant to that of the matrix $\prod_{n=0}^{q-1}[M_1(\tilde{E}_n)]$. Since the eigenvalues are related to the trace via $\mathrm{Tr}[A]=(\alpha+1/\alpha)$, it can be readily shown that, whenever (15) holds, then

$$\left|\mathrm{Tr}\left[\prod_{n=0}^{q-1}[M_1(\tilde{E}_n)]\right]\right|\le\left|\mathrm{Tr}\left[\prod_{n=0}^{q-1}[T_1(E_n)]\right]\right| =|2\cos(\theta q)|<2 .$$

Hence all periodic orbits for the nonlinear lattice chain are linearly stable. Moreover, since for symplectic mappings the linear stability is both necessary and sufficient for nonlinear stability [29,31], the existence of KAM tori close to the periodic orbits is guaranteed for the combined AL-DNLS chain, when $E\mu\ge\gamma$ and $|E|<2$. With the help of this sufficient stability condition we show in

Sec. III below that the reduced two-dimensional (real-valued) map then possesses a stable period-1 orbit which is surrounded by integrable quasiperiodic solutions.

On the other hand, from the stability condition $|\mathrm{Tr}[M_q]|<2$ one can also deduce a necessary condition for the stability of a periodic orbit. The transfer matrix depends parametrically on $\tilde{E}_n$. Therefore, in order to be compatible with $|\mathrm{Tr}[M_q(\tilde{E}_n)]|<2$, we have to distinguish between allowed and forbidden $\tilde{E}_n$, if $\gamma > E\mu$. Because of $\tilde{E}_n=\tilde{E}_n(|\phi_n|)$, *the allowed* $\tilde{E}_n$ *become amplitude dependent,* imposing constraints on the latter. Since each member of a periodic orbit family exhibits the same stability type [29], it is sufficient to consider only one of the periodic points of each family, e.g., $|\mathrm{Tr}M_1(\tilde{E}_n)|<2$. A periodic orbit point is compatible with the allowed E range of the passing band when the amplitude fulfills the necessary condition

$$|\phi_n|^2<\frac{1}{\mu}\left[\left[1+\frac{E-2}{2-\gamma/\mu}\right]^{1/2}-1\right], \tag{21}$$

which reduces to $|\phi_n|^2<(1-E/2)/\gamma$ in the limit $\mu\to 0$. When the condition (21) is violated a stop band (gap) state is encountered.

Generally, whenever the inequality (15) holds, we are able to prove that all solutions of the combined AL-DNLS equation (3) are regular. The linear stability of general orbits (periodic orbits as well as quasiperiodic ones) is governed by a Lyapunov exponent (LE) representing the rate of growth of the amplitudes and is defined as [22,29,32]

$$\lambda=\lim_{N\to\infty}\lambda_N = \lim_{N\to\infty}\frac{1}{2N}\ln\left|\left|\left[\prod_{n=0}^{N}[J(\mathcal{M}_n)]\right]^T\prod_{n=0}^{M}[J(\mathcal{M}_n)]\right|\right| . \tag{22}$$

An orbit is, respectively, linearly stable (unstable) with respect to the initial conditions if $\lambda=0$ ($\neq 0$). It has been proven that almost all initial conditions (except for a set of measure zero) lead to the largest LE [33,34], which in our case is the single non-negative LE, $\lambda\geq 0$. In the parameter range $E\mu\geq\gamma$ and $|E|<2$ we get with the help of inequality (16) and the norm properties $\|A^n\|\leq\|A\|^n$ and $\|AB\|\leq\|A\|\,\|B\|$

$$\begin{aligned}\lambda_N=\frac{1}{2N}\ln\|J_N^T J_N\| &\leq \frac{1}{2N}\ln(\|J_N^t\|\,\|J_N\|)\\ &=\frac{1}{N}\left|\left|\prod_{n=0}^{N}[J(\mathcal{M}_n)]\right|\right|\\ &\leq\frac{1}{N}\prod_{n=0}^{N}\|J(\mathcal{M}_n)\|\leq\frac{1}{N}\ln\|T_1(E)\|^N\\ &=\ln[\max_{\|\varphi=1\|}\|T_1(E)\varphi\|]=0 .\end{aligned} \tag{23}$$

Since λ_N is bounded from above by zero, the LE vanishes,

$$\lambda=0 , \tag{24}$$

and hence *all solutions are linearly stable.* Particularly, sensitive dependence with respect to the initial conditions is excluded so that the combined AL-DNLS system possesses only stable regular orbits, whenever the sufficient condition $E\mu\geq\gamma$ holds. The (local) LE is also directly related to the transmission coefficient in the end of a finite segment of length N of the one-dimensional lattice chain through $\lambda_N=-1/(2N)\ln|T_N|^2$ [35]. In the parameter range given by the inequality (15), the AL-DNLS chain is transparent (see Sec. IV below). We note that in the range outside that of the sufficient condition for regularity ($E\mu\geq\gamma$), and for the special case of constant amplitude $\phi_n=\phi_0$, i.e., for a period-1 cycle, the condition $|\mathrm{Tr}[M_q]|<2$ can be satisfied, if $|\mathrm{Tr}[J(\mathcal{M}_0)]|<2$. Especially, for large amplitudes the trace of all local Jacobians $\tilde{E}_n(|\phi_n|)=\tilde{E}_n(|\phi_0|)$ becomes a constant

$$\lim_{|\phi_0|\to\infty}|\tilde{E}_0|=\frac{\gamma}{\mu} , \tag{25}$$

which implies that, if $\gamma>0$ and $\mu>0$ satisfy the inequality

$$2\mu>\gamma , \tag{26}$$

the global trace is $|\mathrm{Tr}[J(\mathcal{M})]|=|2\cos(N\theta)|<2$, where $\theta=\cos^{-1}[\gamma/(2\mu)]$ and the *large amplitude motion is stable* regardless of E.

B. Application of converse KAM theory

As already stated above, Eq. (1) can be reduced to a real-valued two-dimensional map using the probability current conservation. But, since the resulting map equations [see below Eq. (61) in Sec. III] are not in the appropriate form to allow immediate application of the *converse KAM theory* [29,36,37] it is convenient to cast the complex-valued Eq. (1) into a four-dimensional symplectic twist map $\mathbb{R}^4\to\mathbb{R}^4$, $f(x,y)=(\bar{x},\bar{y})$, by defining $\phi_n=1/\sqrt{2}(Q_n+iq_n)$ and $x=(Q,q)$ together with the canonically conjugate variables $y=(P,p)$ where $P_n=Q_n-Q_{n-1}$ and $p_n=q_n-q_{n-1}$.

We can exploit a variational principle to derive the corresponding map orbits in terms of a Lagrangian system [22,36,37], where each orbit is assigned an action

$$W=\sum_n L(x_n,x_{n+1}) , \tag{27}$$

with the Lagrangian

$$\begin{aligned}L(x_n,x_{n+1})=&\frac{1}{\mu}\left[E-\frac{\gamma}{\mu}\right]\ln\left[1+\frac{1}{2}\mu(Q_n^2+q_n^2)\right]\\ &+\left[\frac{\gamma}{2\mu}-1\right](Q_n^2+q_n^2)+\frac{1}{2}(Q_{n+1}-Q_n)^2\\ &+\frac{1}{2}(q_{n+1}-q_n)^2 .\end{aligned} \tag{28}$$

Stationarity of the action for an orbit requires $\delta W=0$, yielding

$$\frac{\partial}{\partial x_n}[L(x_{n-1},x_n)+L(x_n,x_{n+1})]=0 , \tag{29}$$

and the equations of motion are obtained from

$$y_n=-\frac{\partial L(x_n,x_{n+1})}{\partial x_n},\quad y_{n+1}=\frac{\partial L(x_n,x_{n+1})}{\partial x_{n+1}}\ . \tag{30}$$

The map $f(x,y)=(\bar{x},\bar{y})$ is a twist map since the inner product $\langle \delta y,\partial\bar{x}/\partial y\delta y\rangle=|\delta y|^2$ is uniformly positive [22,36,37].

We now apply the *converse KAM theory* of MacKay, Meiss, and Stark [37] to our four-dimensional map. These authors derived a criterion for the nonexistence of a class of invariant tori for symplectic maps, called Lagrangian graphs. A Lagrangian graph is a set of the form $y=F(x)$ for some C^1 function F and all the invariant tori constructed by most proofs of KAM theory are Lagrangian graphs [38]. In order to apply the converse KAM criterion we collect the necessary definitions and notations for the action principle. The orbits $\{x_i,y_i\}$, $i=m,\ldots,n$ of a symplectic twist map f have stationary action, i.e., $DW_{mn}=0$ under variations by fixing x_m,x_n for all $m<n-1$. If an orbit segment minimizes W_{mn}, it is said to have minimal action. An orbit segment has a nondegenerate minimal action if the second variation δ^2W_{mn} with respect to (x_i), $i=m+1,\ldots,n-1$ is positive definite and an orbit has minimal action if each finite segment has minimal action [22,36,37].

The converse KAM criterion is based on a theorem by Herman [39], stating that for a symplectic twist map every orbit on an invariant Lagrangian graph has minimal action. From this theorem one conversely concludes that if the orbit has a segment which does not have nondegenerate minimal action, then it does not lie on any invariant Lagrangian graph [37]. MacKay *et al.* developed a simple test for the positive definiteness of the second variations $\delta^2W_{-1,n}$ which we apply in the following to our four-dimensional map.

The elements of the second-order variation matrices $a^n=L_{11}(n,n+1)+L_{22}(n-1,n)$ and $b^n=L_{12}(n,n+1)$, where $[n,n+1]$ stands for (x_n,x_{n+1}) and the subscript refers to the derivative with respect to the kth argument, are given by

$$\begin{aligned}(a^n)_{11}=&\frac{1}{[1+\frac{1}{2}\mu(Q_n^2+q_n^2)]^2}\\&\times\{(E-2)[1+\tfrac{1}{2}\mu(q_n^2-Q_n^2)]\\&+(\tfrac{1}{2}\gamma-\mu)[3Q_n^2+q_n^2+\tfrac{1}{2}\mu(Q_n^2+q_n^2)^2]\}+2\ ,\end{aligned} \tag{31}$$

$$(a^n)_{22}=(a^n)_{11}[Q_n\leftrightarrow q_n]\ , \tag{32}$$

$$(a^n)_{12}=(a^n)_{21}=\frac{1}{[1+\frac{1}{2}\mu(Q_n^2+q_n^2)]^2}(\gamma-E\mu)Q_nq_n\ , \tag{33}$$

and

$$(b^n)_{11}=(b^n)_{22}=-1,\quad (b^n)_{12}=(b^n)_{21}=0\ . \tag{34}$$

The existence of an invariant Lagrangian graph requests that it intersects the vertical symmetry plane of $Q_n=q_n$. Therefore a^0 must be positive definite on that plane. Since a symmetric 2×2 matrix is positive definite if both its diagonal elements and its determinant are positive, we obtain the following necessary condition for the existence of an invariant Lagrangian graph through the (initial) point $Q_0=q_0$:

$$Q_0^2=q_0^2\ge\frac{1}{\mu}\left[\left[1+\frac{|E|\mu}{\gamma}\right]^{1/2}-1\right],\quad E<0,\ \gamma>0,\ \mu>0 \tag{35}$$

$$Q_0^2=q_0^2\le\frac{1}{\mu}\left[\left[1+\frac{E\mu}{|\gamma|}\right]^{1/2}-1\right],\quad E>0,\ \gamma<0,\ \mu>0 \tag{36}$$

$$Q_0^2=q_0^2\le\frac{1}{|\mu|}\left[\left[1+\frac{E\mu}{\gamma}\right]^{1/2}-1\right],\quad E<0,\ \gamma>0,\ \mu<0\ . \tag{37}$$

In the limit $\mu=0$ the conditions reduce to

$$Q_0^2=q_0^2\ge\frac{E}{2|\gamma|},\quad E>0,\ \gamma<0 \tag{38}$$

$$Q_0^2=q_0^2\le\frac{|E|}{2\gamma},\quad E<0,\ \gamma>0\ . \tag{39}$$

Note that for an attractive (repulsive) self-interaction of $\gamma>0$ ($\gamma<0$) the amplitude has to be below (above) a certain value to ensure that an invariant Lagrangian graph exists at all.

The necessary criterion for the existence of an invariant Lagrangian graph through a point in phase space is especially important in studying the stability properties, since once it is violated, the nonexistence of a closed invariant KAM circle for the reduced two-dimensional map is ensured (cf. Sec. III). On the two-dimensional plane the KAM circles act like confinement boundaries for trapping solutions in their interior regions.

C. The anti-integrable limit and localized solutions

In this subsection we apply the concept of the *anti-integrable limit* introduced by Aubry and Abramovici [40,41]. We are particularly interested in the impact of the integrable AL term of Eq. (2) on the formation of breathers, i.e., the occurrence of time-periodic, spatially localized solutions. Recently, MacKay and Aubry have proven the existence of localized solutions in the form of breathers for weakly coupled arrays of oscillators [42].

In order to establish the transition to the anti-integrable limit in Eq. (1), we introduce a hopping parameter t regulating the strength of the coupling between adjacent lattice sites. The spatial behavior of the breathers of the DNLS system can be described by a stationary equation with real amplitude $\phi\in\mathbb{R}$ [42]. The action for the real-valued AL-DNLS system now reads

$$F=\sum_n\left\{\frac{1}{2\mu}\left[E-\frac{\gamma}{\mu}\right]\ln(1+\mu\phi_n^2)+\frac{\gamma}{2\mu}\phi_n^2-\frac{t}{2}(\phi_{n+1}-\phi_n)^2\right\}. \tag{40}$$

The map orbits are determined by

$$t(\phi_{n+1}+\phi_{n-1}-2\phi_n)=\frac{E+\gamma\phi_n^2}{1+\mu\phi_n^2}\phi_n \ . \tag{41}$$

The anti-integrable limit for the AL-DNLS system is obtained for vanishing hopping parameter $t=0$, where the action is represented as the sum over local on-site potentials $V(\phi_n)$:

$$F_{AI}=\sum_n \left\{ \frac{1}{2\mu}\left[E-\frac{\gamma}{\mu}\right]\ln(1+\mu\phi_n^2)+\frac{\gamma}{2\mu}\phi_n^2 \right\} \tag{42}$$

$$\equiv \sum_n V(\phi_n) \ . \tag{43}$$

The orbits for the stationary problem are determined by

$$\frac{\partial V(\phi_n)}{\partial \phi_n}\equiv V'(\phi_n)=0 \ , \tag{44}$$

yielding

$$\tilde{\phi}_0=0, \quad \tilde{\phi}_\pm=\pm\sqrt{-E/\gamma}, \quad E<0, \quad \gamma>0 \ . \tag{45}$$

Since orbit points at sites $n+1$ and n are mutually independent of each other an orbit can be associated with an arbitrary sequence of three symbols assigned to $(\tilde{\phi}_0,\tilde{\phi}_\pm)$. Hence the orbits are trivially equivalent to a Bernoulli shift establishing the existence of chaotic orbits [40,41]. We can prove that some chaotic solutions of the anti-integrable limit persist, if the hopping parameter t does not exceed a critical value $t_{\rm crit}$.

Theorem. For

$$t_{\rm crit}\le \frac{|V'(|u_\pm|)|}{4|2\tilde{\phi}_\pm-u_\pm|} \tag{46}$$

there exists a unique solution of Eq. (41) such that for all n

$$|\phi_n-\tilde{\phi}_\pm|\le\delta_\pm=|\tilde{\phi}_\pm-u_\pm| \ , \tag{47}$$

$$|\phi_n-\tilde{\phi}_0|\le\delta_0 \ , \tag{48}$$

with

$$u_\pm=\pm\left\{\frac{1}{2\gamma}\left\{\left[E-3\frac{\gamma}{\mu}\right]+\left[E^2+\left[3\frac{\gamma}{\mu}\right]^2-10E\frac{\gamma}{\mu}\right]^{1/2}\right\}^{1/2}\right\}^{1/2} , \tag{49}$$

$$\delta_0=\left\{\frac{\left|3\frac{\gamma}{\mu}-E+8t\right|}{2\mu\left[\frac{\gamma}{\mu}+4t\right]}\times\left[1+\left[1+4|E+4t|\frac{\left[\frac{\gamma}{\mu}+4t\right]}{\left[3\frac{\gamma}{\mu}-E+8t\right]^2}\right]^{1/2}\right]\right\}^{1/2} , \tag{50}$$

and $(3\gamma)/\mu-E+8t<0$.

Proof. Equation (41) can be rewritten as

$$t(\phi_{n+1}+\phi_{n-1}-2\phi_n)=V'(\phi_n) \ . \tag{51}$$

From (47) we obtain that

$$\sup_n|\phi_{n+1}+\phi_{n-1}-2\phi_n|\le 4|2\tilde{\phi}_\pm-u_\pm| \ , \tag{52}$$

which yields

$$4t|2\tilde{\phi}_\pm-u_\pm|\ge|V'(\phi_n)| \ . \tag{53}$$

When

$$t_{\rm crit}<\frac{\max_n|V'(\phi_n)|}{4|2\tilde{\phi}_\pm-u_\pm|}=\frac{|V'(|u_\pm|)|}{4|2\tilde{\phi}_\pm-u_\pm|} \ , \tag{54}$$

then Eq. (41) has infinitely many solutions. But, in each interval given by the inequalities (47) and (48), there is one and only one solution and hence the problem is uniquely defined.

Sketching the graph of $V''(\phi_n)$ it can be readily seen that $V''(\phi_n)>0$ in the interval given by (47). Further, when (48) holds then $V''(\phi_n)<-4t$. The Jacobian operator D^2F is tridiagonal with diagonal elements $V''+2t$ and off-diagonal elements $-t$. Since $|V''+2t|<2t$, the operator D^2F is invertible and its inverse is bounded. Hence it follows from the implicit function theorem that an orbit has a locally unique continuation for small t [40–45]. ■

It can be easily shown that $\partial t_{\rm crit}/\partial\mu<0$ and $\partial|\delta_{\pm,0}|/\partial\mu<0$. From this we note that the presence of the integrable AL term has a destabilizing influence on the continuation process of the solutions of the anti-integrable limit in the sense that, for higher μ values the continuation can be carried out up to lower t values. Moreover, the amplitudes of the continued solutions decrease with increasing μ. This is immediately reflected in a decreased stability of the breathers, especially for those for which all but one site is unexcited (one-site breathers).

III. REDUCTION OF THE DYNAMICS TO A TWO-DIMENSIONAL MAP

A. The mapping of the plane

We now study the dynamics of Eq. (1) utilizing a planar nonlinear dynamical map approach. The discrete nonlinear Schrödinger equation (1) gives a recurrence relation $\phi_{n+1}=\phi_{n+1}(\phi_n,\phi_{n-1})$ acting as a four-dimensional mapping $\mathbb{C}^2\to\mathbb{C}^2$. By exploiting the conservation of probability current, the dynamics can be reduced to a two-dimensional mapping on the plane $\mathbb{R}^2\to\mathbb{R}^2$ [17,18]. Following Wan and Soukoulis [18], we use polar coordinates for ϕ_n, i.e., $\phi_n=r_n\exp(i\theta_n)$, and rewrite Eq. (3) equivalently as

$$r_{n+1}\cos(\Delta\theta_{n+1})+r_{n-1}\cos(\Delta\theta_n)=\frac{E+\gamma r_n^2}{1+\mu r_n^2}r_n \ , \tag{55}$$

$$r_{n+1}\sin(\Delta\theta_{n+1})-r_{n-1}\sin(\Delta\theta_n)=0 \ , \tag{56}$$

where $\Delta\theta_n=\theta_n-\theta_{n-1}$. Equation (56) is equivalent to conservation of the probability current

$$J=r_n r_{n-1}\sin(\Delta\theta_n) . \tag{57}$$

We further introduce real-valued SU(2) variables defined by bilinear combinations of the wave amplitudes on each "dimeric" segment of the lattice chain:

$$x_n=\phi_n^*\phi_{n-1}+\phi_n\phi_{n-1}^*=2r_n r_{n-1}\cos(\Delta\theta_n) , \tag{58}$$

$$y_n=i[\phi_n^*\phi_{n-1}-\phi_n\phi_{n-1}^*]=2J , \tag{59}$$

$$z_n=|\phi_n|^2-|\phi_{n-1}|^2=r_n^2-r_{n-1}^2 . \tag{60}$$

The relations with the polar coordinates (r_n,θ_n) are also given. Note that the variable y_n is a conserved quantity since it is proportional to the probability current, i.e., $y_n\equiv 2J$. The variable z_n is determined by the difference of the amplitudes of adjacent lattice sites whereas information about the phase difference is contained in the variable x_n. We remark that our map variables differ from those used by Wan and Soukoulis [18] in their study of the stationary DNLS system.

The system of Eqs. (55) and (56) can be rewritten as a two-dimensional real map M that describes the complete dynamics:

$$M:\begin{cases} x_{n+1}=\dfrac{E+\frac{1}{2}\gamma(w_n+z_n)}{1+\frac{1}{2}\mu(w_n+z_n)}(w_n+z_n)-x_n \\ z_{n+1}=\dfrac{1}{2}\dfrac{x_{n+1}^2-x_n^2}{w_n+z_n}-z_n , \end{cases} \tag{61}$$

with $w_n=\sqrt{x_n^2+z_n^2+4J^2}$.

The map M is invertible, proven by the identities $MM_1MM_1=Id$ and $M_1M_1=Id$, where the map M_1 is

$$M_1:\begin{cases} \hat{x}=x \\ \hat{z}=-z . \end{cases} \tag{62}$$

We can cast the map M into the product of two involutions $M=AB$ with $A=M_1M^{-1}$ and $B=M_1M_2$, and $A^2=I$, $B^2=I$, and M_2 is

$$M_2:\begin{cases} \hat{x}=x \\ \hat{z}=z . \end{cases} \tag{63}$$

The inverse map is then given by $M^{-1}=BA$. This invertibility property of the map A can be exploited in studying the transmission properties of the discrete nonlinear chain (see Sec. IV).

To analyze the dynamical properties of the nonlinear map M it is convenient to introduce the scaling transformations $2Jx_n\to\bar{x}_n$, $2Jz_n\to\bar{z}_n$, $J\gamma\to\bar{\gamma}$, and $J\mu\to\bar{\mu}$. Finally, for the sake of simplicity of notation, we drop the overbars and obtain the scaled map

$$x_{n+1}=\frac{E+\gamma(w_n+z_n)}{1+\mu(w_n+z_n)}(w_n+z_n)-x_n , \tag{64}$$

$$z_{n+1}=\frac{1}{2}\frac{x_{n+1}^2-x_n^2}{w_n+z_n}-z_n , \tag{65}$$

with $w_n=\sqrt{x_n^2+z_n^2+1}$.

The map M depends on three parameters, namely, (E,γ,μ). Whereas for $E\mu\geq\gamma$, M represents a map, for which all solutions are bounded, it can contain bounded and diverging orbits both in the pure DNLS case ($\gamma\neq 0$ and $\mu=0$) as well as in the combined AL-DNLS case, if $\gamma>2\mu$ according to the findings in Sec. I. Only the bounded orbits correspond to transmitting waves, whereas the unbounded orbits correspond to waves with amplitude escaping to infinity and hence do not contribute to wave transmission. On inspection we find the first integral for the AL system to be

$$[(x_{n+1}+x_n)^2-K][\mu(x_{n+1}^2-x_n^2)+2(z_{n+1}+z_n)]^2 = E^2(x_{n+1}^2-x_n^2)^2 , \tag{66}$$

where K is a constant determined by the initial conditions.

The structure on the phase plane is organized by a hierarchy of periodic orbits surrounded by quasiperiodic orbits. The sets of the corresponding fixed points form the invariant sets of the two involutions (fundamental symmetry lines) and are given by

$$S_0: z=0 , \tag{67}$$

$$S_1: x=\frac{1}{2}\frac{E+\gamma(w+z)}{1+\mu(w+z)}(w+z) , \tag{68}$$

respectively. The symmetric periodic orbits are arranged along higher-order symmetry lines and the intersection of any two symmetry lines $S_0^n=M^nS_0$, $S_1^n=M^nS_1$ with $n=0,1,\ldots,$ falls on a periodic orbit of M. The symmetry line $z=0$ is the dominant symmetry line and contains at least one point of every positive residue Poincaré-Birkhoff orbit. The organization of the periodic orbits by the symmetry lines can be exploited for a one-dimensional search to locate any desired periodic orbit on the x-z plane [29,46]. For a classification of the periodic orbits Greene's method can be used according to which the stability of an orbit of period q is determined by its residue $\rho=\frac{1}{4}(2-\mathrm{Tr}[\prod_{n=1}^{q}DM^{(n)}])$, where DM is the linearization of M. The periodic orbit is stable when $0<\rho<1$ (elliptic) and unstable when $\rho>1$ (hyperbolic with reflection) or $\rho<0$ (hyperbolic) [29,47].

As can be seen from the determinant of the Jacobian,

$$\det(DM^{(n)})=1+\frac{1}{2}\frac{x_{n+1}^2-x_n^2}{w_n(w_n+z_n)} , \tag{69}$$

the map M is area preserving for periodic orbits, after mapping through the complete period, i.e., $\prod_{n=1}^{q}\det(DM^{(n)})=1$. M is thus topologically equivalent to an area-preserving map ensuring the existence of KAM tori near the symmetric elliptic fixed points [31].

B. Period-doubling bifurcation sequence

We focus on the period-1 orbits (fixed points of M) which have in the case of elliptic-type stability the largest basins of stability among all elliptic orbits. Thus the stable elliptic solutions encircling the fixed point form the main island on the map plane, which therefore plays a major role in determining the stability properties of the

wave amplitude dynamics.

The period-1 orbit is determined by

$$\bar{x}=\frac{1}{2}\frac{E+\gamma\bar{w}}{1+\mu\bar{w}}\bar{w}\ , \tag{70}$$

$$\bar{z}=0\ , \tag{71}$$

where $\bar{w}=\sqrt{1+\bar{x}^2}$. Equation (70) possesses one real root for $\gamma=0$, resulting in a stable elliptic fixed point and has either no root or two real roots for $\gamma>0$. The two real roots correspond to one hyperbolic and one elliptic fixed point, respectively. The residue is given by

$$\rho=1-\frac{1}{4}\frac{(E+\gamma\bar{w})(E+2\gamma\bar{w}+\gamma\mu\bar{w}^2)}{(1+\mu\bar{w})^3}\ . \tag{72}$$

When $\gamma=E\mu$, we recover the degenerate linear case, for which $\bar{x}=\mathrm{sgn}(E)\sqrt{E^2/(4-E^2)}$ and $\rho=1-E^2/4$, as in the genuine linear case $\gamma=\mu=0$.

Figure 1 displays for given nonlinearity parameters μ and γ the location of the fixed points $\bar{x}$ versus E. For the pure DNLS case ($\mu=0$ and $\gamma>0$), shown in Fig. 1(a), we see that the larger the nonlinearity strength γ the more restricted the $\bar{x}$ interval as well as the E range for the existence of the fixed points become. We further observe a bifurcation of the unstable hyperbolic branch (dashed line) into a stable elliptic branch (solid line), which results

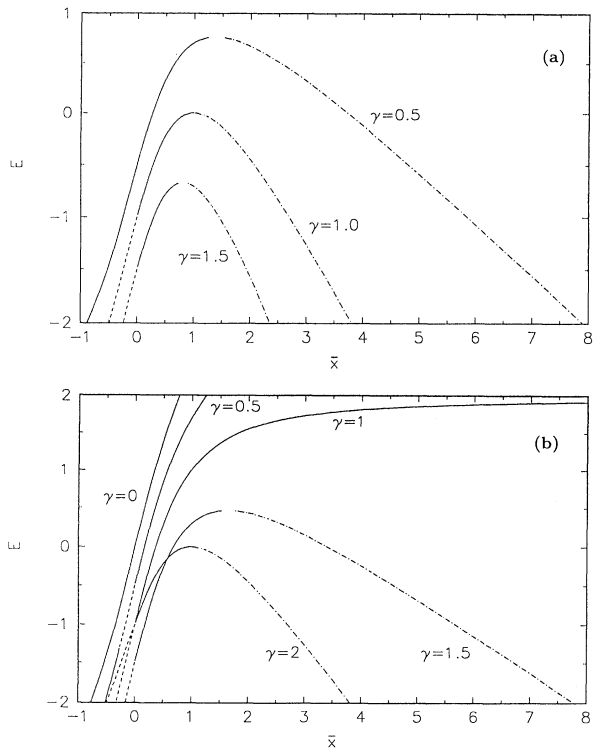

FIG. 1. E versus location of the fixed points $\bar{x}$ of the map M of Eqs. (64) and (65) determined by Eqs. (70) and (71). The solid lines represent stable elliptic-type solutions, the dashed dotted lines correspond to hyperbolic points, and the dashed lines belong to hyperbolic points with reflection. (a) the DNLS case of $\mu=0$ and γ as indicated on the curves. (b) The combined AL-DNLS case of $\mu=0.5$ and γ as curve parameter.

from a reversed pitchfork bifurcation [apparent in Fig. 1(a) for the parameter values $\gamma=1.0$ and 1.5]. Figure 1(b) shows the E-$\bar{x}$ plane for the AL-DNLS case for different γ values and $\mu=0.5$. A comparison with the pure DNLS case shows that the presence of the μ nonlinearity has a stabilizing effect, in the sense that the unstable hyperbolic branch has been shifted towards larger $\bar{x}$ values. Furthermore, we observe that in the $(\mu=0.5,\gamma=1.0)$ case, the fixed points become stable elliptic points in the whole $\bar{x}$ range of their existence, hence no bifurcation occurs, on contrast to the bifurcation behavior for the corresponding $(\mu=0,\gamma=1.0)$ case.

Concerning the stability of the period-1 orbit, Eq. (72) tells us that the residue remains positive and never passes through zero, if the parameters obey the inequalities $\gamma<E_\mu$ and $|E|<2$. As a result, the period-1 orbit cannot lose stability caused by a tangent bifurcation. According to the results obtained in Sec. I, all orbits of the map are regular in this parameter range.

Equation (72) allows a further conclusion to be drawn: For $E>0$ the value of the residue for the period-1 orbit is always less than one, because the second term on the right-hand side then remains positive upon parameter changes and the position of the fixed point is merely shifted and never experiences loss of stability due to a period-doubling bifurcation. In this parameter range the route to global chaos is via resonance overlap. Only for $E<0$ can the residue pass the value of one connected with the onset of a period-doubling bifurcation, where the stable fixed point is converted into an unstable hyperbolic point with reflection accompanied by the creation of two additional elliptic points. This period-doubling bifurcation for the period-1 orbit sets in when $|E|/\gamma>1$ $(E<0)$ and the newborn period-2 orbits are located at

$$x=\pm\left[\left[\frac{E}{\gamma}\right]^2-1\right]^{1/2}\ , \tag{73}$$

$$z=0\ . \tag{74}$$

Note that the location of the period-2 orbits depends only on the (E,γ) values and is independent of μ, the AL-nonlinearity strength, whereas their stability, determined by the corresponding residue

$$\rho=\frac{1}{2}\gamma^2\frac{E^2-\gamma^2}{(\gamma+\mu|E|)^2}\ , \tag{75}$$

depends on the values of all three parameters. Due to the presence of the denominator in Eq. (75) we recognize that, for fixed parameters (E,γ), enhancing the μ value reduces the residue. Hence the period-2 orbits become more resistant with respect to period-doubling bifurcation. Moreover, for $\mu>\mu_c$ the value for the residue of the two stable elliptic points is bounded from above by one, so that a further destabilizing bifurcation can be excluded. This critical AL-nonlinearity strength $\mu_c(\rho<1)$ can be obtained as

$$\mu_c>\left\{\frac{1}{2}\gamma^2\left[1-\left[\frac{\gamma}{E}\right]^2\right]\right\}^{1/2}-\frac{\gamma}{|E|}\ . \tag{76}$$

To study the period-doubling sequence as the mecha-

nism by which the transition from regular to chaotic motion occurs, we take advantage of the renormalization technique developed for two-dimensional invertible maps [29,46,48–50]. We expand the map M up to terms quadratic in the deviation from the bifurcation point

$$\begin{bmatrix} \delta u_{n+1} \\ \delta v_{n+1} \end{bmatrix} = \mathcal{A} \begin{bmatrix} \delta u_n \\ \delta v_n \end{bmatrix} + \mathcal{B} \begin{bmatrix} \delta u_n^2 \\ \delta u_n \delta v_n \\ \delta v_n^2 \end{bmatrix} . \tag{77}$$

The 2×2 matrix $\mathcal{A}$ has the following entries:

$$\mathcal{A}_{11}=-1, \quad \mathcal{A}_{12}=\frac{E+2\gamma+\mu\gamma}{[1+\mu]^2} ,$$
$$\mathcal{A}_{21}=-\frac{E+\gamma}{1+\mu}, \tag{78}$$
$$\mathcal{A}_{22}=\frac{1}{2}\frac{[E+\gamma][E+3\gamma+\gamma\mu-E\mu]}{[1+\mu]^3}-1 ,$$

and the elements of the 2×3 matrix $\mathcal{B}$ are given by

$$\mathcal{B}_{11}=\mathcal{A}_{12}, \quad \mathcal{B}_{12}=0 ,$$
$$\mathcal{B}_{21}=\mathcal{A}_{22}+1, \quad \mathcal{B}_{22}=\mathcal{A}_{12} ,$$
$$\mathcal{B}_{13}=\frac{E+4\gamma+3\gamma\mu-E\mu+\gamma^2\mu^2}{[1+\mu]^3} , \tag{79}$$
$$\mathcal{B}_{23}=\frac{1}{2}\frac{E^2+8\gamma-4E\gamma\mu+9\gamma^2+\gamma^2\mu^2-4E^2\mu+\mu^2E^2}{[1+\mu]^4} .$$

Finally, we bring the De Vogelaere–type map (77) into the standard form of a closed second-order difference equation (see Ref. [48] for the details of how to achieve this form):

$$Q_{n+1}+Q_{n-1}=CQ_n+2Q_n^2 , \tag{80}$$

where the parameter C is determined via the sum of the eigenvalues of the matrix $\mathcal{A}$:

$$C=\frac{1}{4}\frac{[E+\gamma][E+3\gamma+\gamma\mu-E\mu]}{[1+\mu]^3}-1 . \tag{81}$$

The fixed point of Eq. (80) at $\bar{Q}=0$ is stable for $|E|/\gamma<1$ and gets unstable for $3>|E|/\gamma>1$, leading to a period-doubling bifurcation. Both points of the newborn period-2 orbit are located on the S_0-symmetry line, along which they get shifted upon increasing $|E|$. Eventually, at a sufficiently high $|E|$ value the period-2 orbit also loses stability caused by a next period-doubling bifurcation, which in turn gives rise to the birth of the corresponding period-4 orbit having one point on the S_1-symmetry line and two points on the S_0-symmetry line. For further increased $|E|$ the period-4 orbit also goes unstable in the next step of the period-doubling cascade.

This cascade of period-doubling bifurcations terminates at a universal critical parameter C_∞, called the accumulation point, where local chaos appears. Employing a quadratic renormalization scheme for Eq. (80), this accumulation point has been determined to be $C_\infty\approx -1.2656$ [29,46,48–50]. Solving Eq. (81) for $E_\infty=E(\gamma,\mu,C_\infty)$ we obtain

$$E_\infty=-\frac{1}{1-\mu}[2\gamma+(1+\mu)\sqrt{\gamma^2-|C_\infty|(1-\mu^2)}] . \tag{82}$$

Apparently, for a given DNLS-nonlinearity strength γ, we conclude that enhancing the AL-nonlinearity strength μ results in an increase of the accumulation value $|E_\infty|$ (provided $\mu<1$), i.e., *the μ term has the stability tendency to prevent period-doubling sequences.*

In Fig. 2(a) we show a number of orbits of the map M for $E=0.5$, $\gamma=0.2$, and $\mu=0.1$ together with the symmetry lines S_0 and S_1. This map exhibits a rich structure involving regular quasiperiodic (KAM) curves which densely fill the large basin of attraction of the stable period-1 orbit. The elliptic fixed points of the Poincaré-Birkhoff chains of various higher-order period orbits are also surrounded by regular KAM curves, while thin chaotic layers develop in the vicinity of the separatrices of the corresponding hyperbolic fixed points. Moreover, outside the structured core containing trapped trajectories inside the resonances, a broad chaotic sea has been developed where the corresponding unstable orbits may escape to infinity. For comparison we illustrate in Fig. 2(b) the integrable behavior for the AL map where the corresponding orbits can be generated from Eq. (66). In Fig. 2(c) we show the case for which $E\mu\geq\gamma$, i.e., when the condition of Eq. (15) for regular solutions is fulfilled, whereas the case with $E<0$ but $2\mu>\gamma$ is shown in Fig. 2(d). We note that in the latter case all solutions are bounded.

In order to study the global stability properties of the map M, we plotted in Fig. 3 the stability diagram in the x_0-E plane. For a set of initial conditions located on the dominant symmetry line, i.e., $z=z_0=0$ and various $x=x_0$, we iterated the map equations (64) and (65). The dark region in Fig. 3 corresponds to stable solutions where the resulting orbit remains in a bounded region on the x-z plane of the map, whereas the white region on the x_0-E plane represents unbounded orbits. The curve separating the two regimes exhibits a rich structure. Practically, all lines of constant E pass several branches of either transmitting or nontransmitting solutions, indicating multistable behavior. Multistability in the wave transmission along the nonlinear lattice chain will be considered in more detail in the next section.

We further note that with increasing AL-nonlinearity parameter μ the area of transmitting solutions on the E-x_0 plane is enhanced. This stabilizing effect of larger μ values is clearly seen in Figs. 3(c) and 3(d), where the region for stable propagating solutions is not only further extended to the range of negative E values, but also covers a wider range for the initial amplitudes x_0. Beyond a certain nonlinearity strength $\mu\geq\gamma/E$, the nonlinear lattice chain eventually becomes transparent for all amplitudes.

In Figs. 3(a) and 3(b) we also superimposed the lines for the location of the fixed point (period-1 orbit) of the map M. Following that line the occurring transition from a bounded to an unbounded regime for initial conditions around the period-1 orbit is a consequence of stability loss when passing from elliptic-type stability to hyperbolic-type instability upon changing E. Due to the

results for the stability of the period-1 orbits contained in Fig. 1 they may experience a bifurcation from an unstable hyperbolic fixed point to a stable elliptic fixed point by increasing E where the corresponding x_0 values then come to lie in the basin of attraction of the elliptic point. At a critical E value the initial conditions x_0 leave the basin of attraction of the elliptic point and fall into the range of the unstable reflection hyperbolic point. Between the lower and the upper stability boundaries the elliptic point loses its stability temporarily, caused by a quadrupling bifurcation where the corresponding residue is $\rho=0.75$, leading to a local shrinkage of the area for bounded solutions which appears in Fig. 3(a) for $E\simeq -1.075$ and $x_0\simeq 0.24$.

IV. TRANSMISSION PROPERTIES

In this section we study as a physical application the wave transmission properties of the nonlinear lattice chain. Our aim is to gain more insight into the effects of the combined AL-nonlinearity term and the DNLS-nonlinearity term with regard to wave transparency of a finite nonlinear segment embedded in a linear chain.

A. Amplitude stability

We study the following transmission problem: Plane waves with momentum k are sent from the left towards the nonlinear chain, where they will be scattered into a reflected and transmitted part:

$$\phi_n=\begin{cases} R_0\exp(ikn)+R\exp(-ikn) & \text{for } 1\le n\le N \\ T\exp(ikn) & \text{for } n\ge N\ . \end{cases}$$

We denote by R_0,R the amplitudes of the incoming and reflected waves and by T the transmitted amplitude at the right end of the nonlinear chain. The wave number k is in the interval $[-\pi,\pi]$ yielding $|E|\le 2$.

Since the superposition principle is no longer valid in the nonlinear case, the transmitted amplitude T is not uniquely defined by the incident amplitude R_0. To circumvent this difficulty we solve the inverse transmission problem, i.e., we compute the input amplitude R_0 for fixed output amplitude T (see also [17]). The procedure relies on the inverse map given by $M^{-1}=M_1\circ M\circ M_1$ which we interpret as "backward map" in the following manner. For a given output plane wave with transmitted intensity T at the right end of the nonlinear chain we have $(\phi_{N+1},\phi_N)=[T\exp[ik(N+1)],T\exp(ikN)]$.

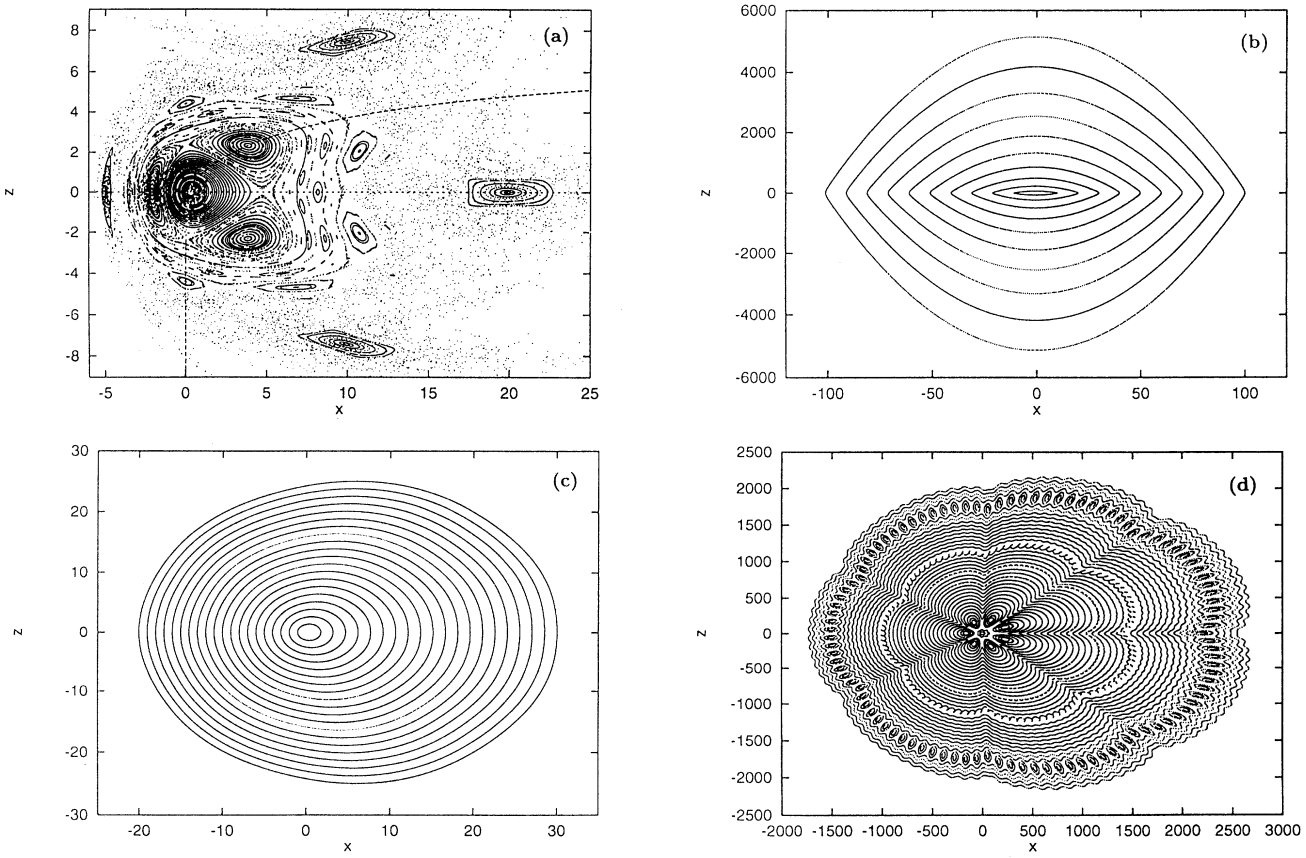

FIG. 2. Orbits of the map M given in Eqs. (64) and (65) for the following parameters: (a) AL-DNLS case: $E=0.5$, $\gamma=0.2$, and $\mu=0.1$; (b) AL case: $E=-1.0$, $\gamma=0$, and $\mu=1.0$; (c) regular regime: $E=1.0$, $\gamma=0.2$, and $\mu=0.25$; and (d) bounded regime: $E=-1.7$, $\gamma=0.5$, and $\mu=1.1$. The fundamental symmetry lines S_0 and S_1 are superimposed.

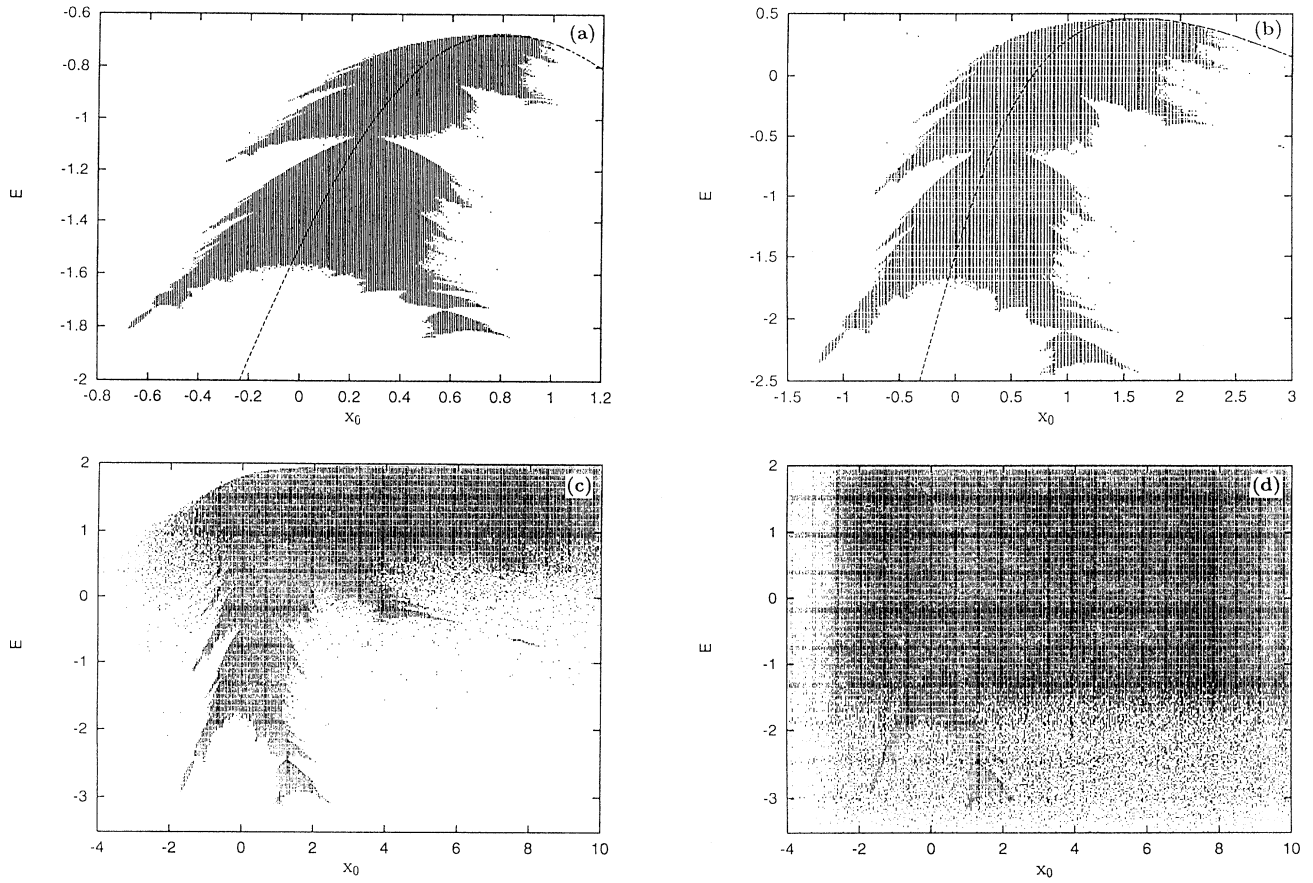

FIG. 3. Illustration of the stability behavior of the map M with $\gamma=1.5$ in the E-x_0 parameter plane. Bounded solutions correspond to the dark areas whereas diverging solutions are indicated by the white area (see text). The AL-nonlinearity strength μ is (a) $\mu=0$, (b) $\mu=0.5$, (c) $\mu=0.75$, and (d) $\mu=0.76$.

From the pair (ϕ_{N+1},ϕ_N) we obtain (r_{N+1},r_N) and (θ_{N+1},θ_N) as well as $(x_{N+1}=2|T|^2\cos(k),z_{N+1}=0)$. The latter are used as initial conditions for the map M^{-1} in the study of the fixed output transmission problem. For a given wave number k the current J is fixed through the expression $J=|T|^2\sin(k)$. We see therefore that the pair $(k,|T|)$ initializes the map M^{-1} completely. Iterating the map M^{-1} from $n=N$ to 0 successively determines the amplitudes $(r_{N-1},\ldots,r_0)$ and phases $(\theta_{N-1},\ldots,\theta_0)$ and eventually results in the value of ϕ_0 on the left end of the nonlinear chain.

Figure 4 displays the transmission behavior in the k-$|T|$ parameter plane (momentum versus intensity amplitude of an outgoing wave), showing regions of transmitting (white) and nontransmitting (hatched) behavior. This representation is similar to that used by Delyon, Levy, and Souillard and Wan and Soukoulis in the study of the corresponding stationary DNLS model [17,18].

For a given output wave with intensity $|T|$ and momentum k the inverse map M^{-1} has been iterated by taking a grid of 500 values of k and 250 values of $|T|$. Correspondingly, to initialize the map M^{-1} we populate

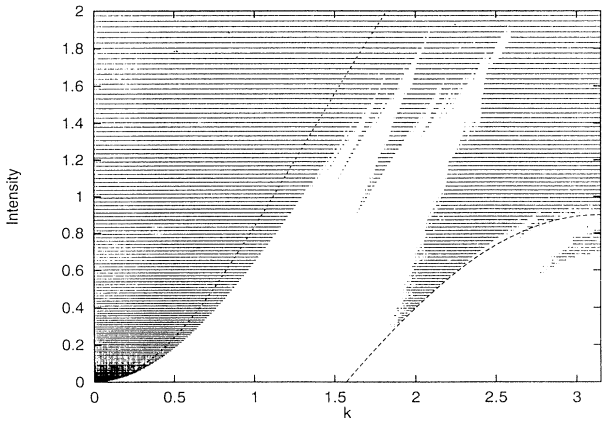

FIG. 4. Wave transmission properties in the intensity versus momentum k plane. Hatched regions correspond to the nontransmitting regime whereas the white regions indicate transmission. The chain length is $N=200$. We show the AL-DNLS case $\gamma=1.0$ and $\mu=0.25$. The dashed curves represent the boundary between nonescaping and escaping solutions obtained analytically from Eqs. (83) and (84).

the z axis with initial conditions $x_0=2|T|\cos(k)$, $z_0=0$ and iterate on each individual point. When the resulting incoming wave intensities $|R_0|$ are of the same order of magnitude as the transmitted intensity, the nonlinear chain is said to be transmitting (white area in Fig. 4). In Fig. 4 we show the AL-DNLS case $\mu=0.25$, with $\gamma=1$.

For wave numbers $|k|\in[\pi/2,\pi]$, where the map M has no fixed point at all, the regions of bounded and unbounded solutions are separated by a sharp smooth curve which can be obtained approximately from the analysis for the initial wave amplitude stability performed in Sec. II. Using Eq. (21) the boundary follows from

$$|\phi_T|^2=\frac{1}{\mu}\left\{\left[1+\frac{2\mu[1-\cos(k)]}{\gamma-2\mu}\right]^{1/2}-1\right\}, \tag{83}$$

where ϕ_T is the critical value for the wave amplitude above which stable transmission is necessarily impossible. On the other hand, application of converse KAM theory leads to a necessary condition for the existence of an invariant graph through a given point. According to Eq. (37), there exists no invariant closed KAM circle on the two-dimensional map plane when the wave amplitude exceeds the value

$$|\phi_T|^2=\frac{1}{\mu}\left[\left[1-2\frac{\mu}{\gamma}\cos(k)\right]^{1/2}-1\right], \tag{84}$$

which yields the curve creating the lower boundary curve for the largest instability tongue in Fig. 4.

As AL nonlinearity increases, its stabilizing effect manifests itself in an area enhancement of the region for transmitting solutions. This effect becomes more pronounced for higher AL-nonlinearity strength (not shown here), eventually exhibiting *perfect transmittance,* when $E\mu\geq\gamma$.

For $|k|<\pi/2$ the region for nontransmitting solutions ranges down into the region of linearly transmitting solutions, thus decreasing transparency. The boundary discerning between bounded and unbounded solutions shows a complex structure created by numerous narrow hatched tongues. The white regions between each of these tongues can be assigned to a corresponding stability basin of an elliptic periodic orbit and the fractal structure of the boundary curves originates from the hierarchical, self-similar structure of islands around islands formed by higher-class periodic orbits [17,18].

In the transmission diagrams represented in Fig. 5, several branches are created for $k\in[-\pi/2,\pi/2]$ at critical intensities $|T|$, indicating bistable or multistable behavior. Such multistability is illustrated in Fig. 5, where the transmitted wave intensity is plotted versus the intensity of the incoming wave for $k=0.927$. The curve in Fig. 5(a) illustrating the pure DNLS case ($\gamma=1.0,\mu=0$) shows oscillations resulting in numerous different output energies for a given input energy. Above an output intensity of 0.68, a transmission gap ranging up to 1.08 occurs. Figure 5(b) demonstrates that the presence of a stabilizing AL nonlinearity of $\mu=0.5$ closes the gap, i.e., transmittivity of the nonlinear lattice is restored.

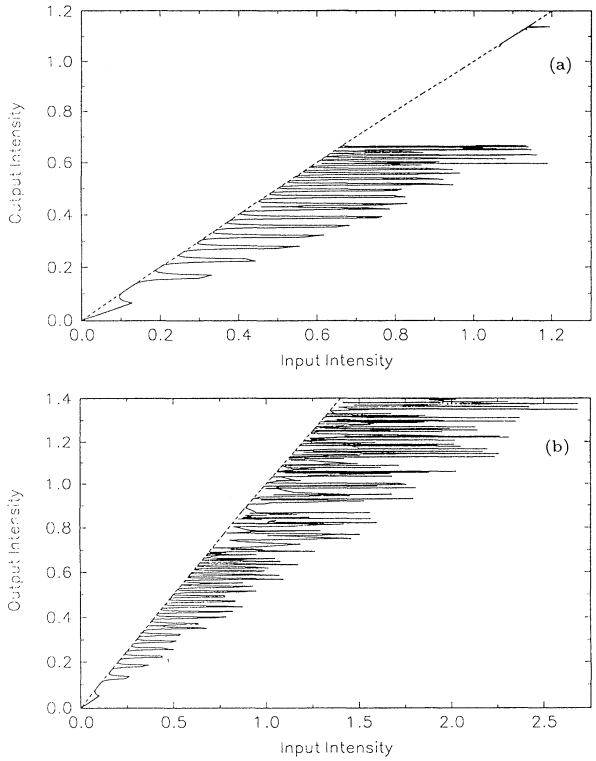

FIG. 5. Transmitted intensity as a function of the incident intensity exhibiting multistability of the nonlinear transmission dynamics for a nonlinear chain consisting of 200 sites. The parameters are $E=-1.2$, $\gamma=1.0$, and (a) $\mu=0$. A transmission gap occurs. (b) The gap has been closed for $\mu=0.5$.

B. Relation to chaotic scattering

The dynamics of the wave amplitude in the range $k\in[-\pi/2,\pi/2]$ is extremely sensitive to the choice of the initial momenta k as well as the initial amplitude. The occurrence of "spatial" chaos can thus be expected in the wave transmission. We want to relate the appearing irregularity in the escape process to the features of chaotic scattering [51–54]. The influence of the chain length of the present nonlinear lattice model on the creation of gap and band states was studied.

To analyze the nonpropagating states, manifested in diverging solutions of the nonlinear discrete Schrödinger equation, we have employed the concept of the *exit time* typical in chaotic scattering studies. The "exit time" measures the number of iterations $N_{\rm esc}$ required to let a characteristic variable exceed some critical escape value. In our case we take the initial amplitude x_0 for the map $M=M(x,z)$ as the input variable and we obtain the escape function by following the growth of $\frac{1}{2}(w_n+z_n)=|\phi_n|^2$. When $|\phi_n|^2$ exceeds a certain threshold (taken to be equal to 500) we register the corresponding value of N as $N_{\rm esc}$.

Figure 6(a) shows $N_{\rm esc}(x_0)$ for $\gamma=1.5$, $\mu=0$, and $E=-1.1$, for 5000 different initial values x_0 arranged on the dominant symmetry line $z=0$ of the map M. The choice of these initial conditions for the map corresponds

to the case of the "forward" scattering problem (fixed input problem), where plane waves with amplitudes R_0 are sent from the left to the nonlinear chain and the relation between the initial map variable and the initial wave amplitude is $x_0 \equiv 2|R_0|^2 \cos(k)$. Except for the two regular windows of no escape in the intervals $-0.2 < x_0 < -0.1$ and $1.8 < x_0 < 4.5$, this escape number function shows rapid oscillations and flat parts, which is a typical feature of *chaotic scattering* [51,53]. The rapidly oscillating parts indicate a sensitive dependence of the escape process on the initial amplitude, whereas in the flat regions the escape number N_{esc} for different initial amplitudes remains approximately constant. An expansion of the scale in Fig. 6(a) reproduces analogous features over many orders of magnitude, i.e., a self-similar structure. The appearance of smooth and wild oscillating parts is due to the fact that the escape function exhibits singularities on a fractal set of initial conditions, which is the hallmark of chaotic scattering.

A possible application of this work in optical wave transmission is worth mentioning [16]. In particular, the onset of the irregular oscillations of Fig. 6(a) determines waveguide lengths (possible operating regimes) for the optically coupled devices, since in these ranges practical prediction of transmitting (nontransmitting) properties is not possible. On the other hand, the regular regions of Fig. 6(a) correspond to waveguide lengths that have determined regular properties and thus can be used reliably for information transmission via amplitude modulation [55].

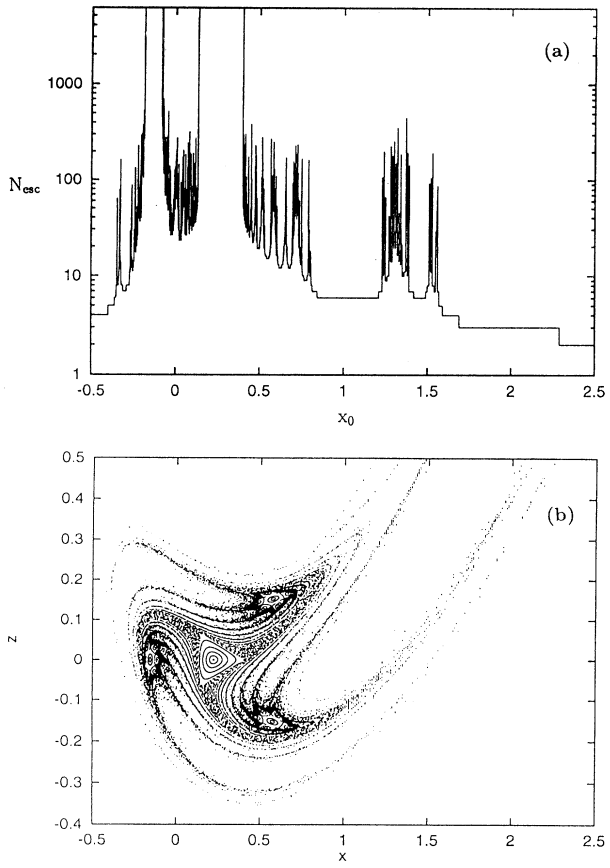

FIG. 6. Illustration of the chaotic scattering properties in the escape process for the wave amplitudes. (a) The escape length N_{esc} as a function of the initial conditions x_0 (for explanation see text). (b) The corresponding orbits of the map M showing the escape set consisting of remnants of KAM curves and unstable manifolds of saddle points and the invariant nonescaping set built up from unbroken KAM curves.

For an understanding of the behavior of the escape number function, we show in Fig. 6(b) the ensemble of those trajectories for the map M from which we constructed Fig. 6(a). KAM islands surrounding the elliptic period-1 orbit, the elliptic period-3 orbit, and also the invariant curves contained in the stable islands associated with the higher-order period orbits around the period-3 islands provide the bounded invariant set of the map. They yield the two windows of no escape for stable propagating states in Fig. 6(a). Conversely, the scattering points of the escaping orbits can never penetrate these KAM circles which act as repellers. The intersections of the stable and unstable manifolds of the unstable saddles create the invariant set responsible for the chaotic scattering. Since there still exist unbroken KAM curves, this set is *nonhyperbolic* [54]. The escaping set, which is the complementary set of the KAM islands, contains a nonhyperbolic set that produces the sensitivity to the initial conditions as well as the remainings of KAM islands. The discontinuity of the escape function is a consequence of Cantor-like structure of the stable and unstable manifolds of the invariant set, whereas the remains of KAM curves in the invariant set are responsible for the flat parts of the escape function. In Fig. 6(b) one clearly recognizes the unstable manifolds of the period-3 saddle as well as those of the higher-order periodic orbit saddles surrounding the period-3 islands. These unstable manifolds extend to infinity and shape the scattering pattern.

V. CONCLUSION

In this paper we presented an investigation of the nonlinear stationary problem of a discrete nonlinear equation that interpolates between the Ablowitz-Ladik and discrete nonlinear Schrödinger equations. We transformed the stationary AL-DNLS equation into a dynamical map problem by associating the lattice indices with discrete time and pairs of amplitudes of adjacent lattice sites with a two-component column vector. As a result, the nonlinear eigenvalue problem of the combined AL-DNLS equation was shown to be equivalent to a two-dimensional nonlinear (locally) area-preserving dynamical map. In the map context, regular bounded orbits correspond to extended periodic or quasiperiodic (transmitting) stationary waves, whereas irregular unbounded orbits correspond to (localized) nonpropagating waves.

The different regimes of the dynamical system were seen to depend on the two nonlinearity parameters μ and γ as well as the wave energy E. Using the properties of the tangent space map we found that, when $E\mu \geq \gamma$ is satisfied, all orbits are characterized by a (largest) Lyapunov exponent that is equal to zero, thus leading to

stable solutions. Consequently, this inequality marks the regime where transmission through the nonlinear lattice is ensured. Furthermore, for waves with energies outside this regime we found that stable map solutions are also guaranteed when $2\mu > \gamma$. The existence of these regular regimes shows that the presence of the AL term in Eq. (1) has the significant function of creating an "integrability regime" for the nonintegrable DNLS equation. This stabilization property of the AL term was also seen in the study of the period-doubling bifurcation sequence that was studied in Sec. III. Quispel, Roberts, and Thompson [21] conjectured that every autonomous difference equation obtained by a stationary reduction of an integrable time-dependent differential-difference equation is an integrable mapping. The converse of this conjecture does not necessarily hold. The integrable (time-dependent) AL equation provides such a system where the stationary equation yields an integrable mapping [cf. Eq. (66)]. Therefore it would be interesting to consider the manifestation of the regular regime obtained in this paper for the stationary combined AL-DNLS equation in the corresponding time-dependent combined equation (2). Work in this direction is in progress [56].

On the other hand, application of the anti-integrable limit showed that the AL contribution in the combined AL-DNLS system has a destabilizing influence on breather solutions.

Finally, we also studied the transmission properties of Eq. (1) in two ways and showed that in addition to the regular transparent regimes, there are also cases where multistability is possible. This property can be used in the context of certain nonlinear coupler applications for efficient transmission of information through the system. First, we used the converse KAM theory to obtain bounds for having stable bounded solutions. These bounds determine the maximal wave amplitude for which stable propagating (transmitting) waves are possible. Subsequently we analyzed the wave transmission problem and compared the transmission with the aforementioned bounds obtained analytically. The effect of the AL term is to close the transmission gaps and thus enhance the transparency of the nonlinear lattice. We finally discussed aspects of the AL-DNLS lattice from the point of view of chaotic scattering and found the possible regimes (chain lengths) at which the chain can be used for reliable information transfer.

In the present work, we used the AL-DNLS equation as a test case in the study of the interplay of integrability and nonintegrability in an extended system. From the point of view of physics, we can relate the AL-DNLS equation to wave propagation in nonlinear core couplers when, in addition to the basic self-interacting term (i.e., the DNLS term) we also have a contribution through a nonlinear coupling of adjacent waveguides (i.e., the AL term) [16]. In this type of optical applications of the AL-DNLS equation an interesting case emerges when periodicity is induced in the system by, for instance, adding a linear periodic local term to Eq. (2). In the simplest case, if a term proportional to $\epsilon\delta_{n,2m}\psi_m(t)$ is added, we have an increase in the size of the unit cell leading to the simplest multiband extension of Eq. (2). It is known that in such cases gap solitons can propagate in the forbidden energy range between the two bands [57–61]. It would be interesting to study the dynamical properties of the discrete analogs of these gap solitons in the context of Eq. (2) and determine the role of the interplay between integrability and nonintegrability.

ACKNOWLEDGMENTS

This work was supported by the Deutsche Forschungsgemeinschaft via Sonderforschungs-bereich 337 and TARP Grant No. 003656-073C. Two of the authors (N.G.S. and G.P.T.) gratefully acknowledge the warm hospitality of the Institut für Theoretische Physik, Freie Universität, Berlin, Germany. The authors thank M. I. Molina for valuable discussions.

[1] M. J. Ablowitz and P. A. Clarkson, *Solitons, Nonlinear Evolution Equations and Inverse Scattering* (Cambridge University Press, New York, 1991).
[2] M. J. Ablowitz and J. F. Ladik, J. Math. Phys. **17**, 1011 (1976).
[3] J. C. Eilbeck, P. S. Lomdahl, and A. C. Scott, Physica D **16**, 318 (1985).
[4] B. M. Herbst and M. J. Ablowitz, Phys. Rev. Lett. **62**, 2065 (1989).
[5] V. M. Kenkre and D. K. Campbell, Phys. Rev. B **34**, 4959 (1986).
[6] A. S. Davydov and N. I. Kislukha, Phys. Status Solidi B **59**, 465 (1973).
[7] N. Finlayson and G. I. Stegeman, Appl. Phys. Lett. **56**, 2276 (1990).
[8] Y. Chen, A. W. Snyder, and D. J. Mitchell, Electron. Lett. **26**, 77 (1990).
[9] M. I. Molina, W. D. Deering, and G. P. Tsironis, Physica D **66**, 135 (1993).
[10] S. Takeno and S. Homma, J. Phys. Soc. Jpn. **60**, 731 (1991); **62**, 835 (1993).
[11] G. S. Zavt, M. Wagner, and A. Lütze, Phys. Rev. E **47**, 4108 (1993).
[12] M. I. Molina and G. P. Tsironis, Phys. Rev. Lett. **73**, 464 (1994).
[13] D. Cai, A. R. Bishop, and N. Grønbech-Jensen, Phys. Rev. Lett. **72**, 591 (1994).
[14] The quantum version of the combined AL-DNLS equation was studied in M. Salerno, Phys. Rev. A **46**, 6856 (1992).
[15] M. H. Hays, C. D. Levermore, and P. D. Miller, Physica D **79**, 1 (1994).
[16] G. P. Tsironis, D. Hennig, and N. G. Sun (unpublished).
[17] F. Delyon, Y.-E. Levy, and B. Souillard, Phys. Rev. Lett. **57**, 2010 (1986).
[18] Yi Wan and C. M. Soukoulis, Phys. Rev. A **41**, 800 (1990); in *Disorder and Nonlinearity*, edited by A. R. Bishop, D. K. Campbell, and S. Pnevmatikos (Springer, New York, 1989), pp. 27–37.
[19] K. A. Ross and C. J. Thompson, Physica A **135**, 551

(1986).
[20] G. R. W. Quispel, J. A. G. Roberts, and C. J. Thompson, Physica D **34**, 183 (1989).
[21] G. R. W. Quispel, J. A. G. Roberts, and C. J. Thompson, Phys. Lett. A **126**, 419 (1988).
[22] S. Aubry, Physica D **7**, 240 (1983).
[23] S. Aubry and P. Y. Le Daeron, Physica D **8**, 381 (1983).
[24] H. A. Kramers, Physica **2**, 483 (1935).
[25] H. M. James, Phys. Rev. **76**, 1602 (1949).
[26] W. Kohn, Phys. Rev. **115**, 809 (1959).
[27] R. E. Borland, in *Mathematical Physics in One Dimension,* edited by E. Lieb and D. C. Mattis (Academic, New York, 1966).
[28] D. R. Hofstadter, Phys. Rev. B **14**, 2239 (1976).
[29] A. J. Lichtenberg and M. A. Liebermann, *Regular and Stochastic Motion* (Springer-Verlag, New York, 1992).
[30] R. Bellman, *Introduction to Matrix Analysis* (McGraw-Hill, New York, 1970).
[31] V. I. Arnold, in *Nonlinear and Turbulent Processes in Physics,* edited by R. Z. Sagdeev (Harwood, Chur, 1984), p. 116.
[32] I. Shimada and T. Nagashima, Prog. Theor. Phys. **61**, 1605 (1979).
[33] V. I. Oseledec, Trans. Mosc. Math. Soc. **19**, 197 (1968).
[34] G. Benettin, L. Galgani, and J.-M. Strelcyn, Phys. Rev. A **14**, 22 338 (1976).
[35] P. D. Kirkman and J. B. Pendry, J. Phys. C **17**, 4327 (1984).
[36] J. D. Meiss, Rev. Mod. Phys. **64**, 795 (1992).
[37] R. S. MacKay, J. D. Meiss, and J. Stark, Nonlinearity **2**, 555 (1989).
[38] V. I. Arnold and A. Avez, *Ergodic Problems of Classical Mechanics* (Benjamin, New York, 1968).
[39] M. R. Herman, Asterisque **103-104**, 1 (1983).
[40] S. Aubry and G. Abramovici, Physica D **43**, 199 (1990).
[41] S. Aubry, Physica D **71**, 196 (1994).
[42] R. S. MacKay and S. Aubry, Nonlinearity **7**, 1623 (1994).
[43] J. J. P. Veerman and F. M. Tangerman, Commun. Math. Phys. **139**, 245 (1991).
[44] R. S. MacKay and J. D. Meiss, Nonlinearity **5**, 149 (1992).
[45] C. Baesens and R. S. MacKay, Physica D **71**, 372 (1994).
[46] R. S. MacKay, Physica D **7**, 283 (1983).
[47] J. Greene, J. Math. Phys. **20**, 257 (1979).
[48] R. H. G. Helleman, in *Nonequilibrium Problems in Statistical Mechanics,* edited by W. Horton, L. Reichl, and V. Szebehely (Wiley, New York, 1981), Vol. 2.
[49] J. Greene, R. S. MacKay, F. Vivaldi, and M. J. Feigenbaum, Physica D **3**, 468 (1981).
[50] T. Bountis, Physica D **3**, 577 (1981).
[51] S. Bleher, E. Ott, and C. Grebogi, Phys. Rev. Lett. **63**, 919 (1989).
[52] G. Troll and U. Smilansky, Physica D **35**, 34 (1989).
[53] M. Ding, C. Grebogi, E. Ott, and J. A. Yorke, Phys. Rev. A **42**, 7025 (1990).
[54] S. Bleher, C. Grebogi, and E. Ott, Physica D **46**, 87 (1990).
[55] D. Hennig, H. Gabriel, G. P. Tsironis, and M. I. Molina, Appl. Phys. Lett. **64**, 2934 (1994).
[56] D. Hennig and G. P. Tsironis (unpublished).
[57] H. G. Winful, Appl. Phys. Lett. **46**, 527 (1985).
[58] W. Chen, and D. L. Mills, Phys. Rev. Lett. **58**, 160 (1987).
[59] D. L. Mills and S. E. Trullinger, Phys. Rev. B **36**, 947 (1987).
[60] J. Coste and J. Peyrard, Phys. Rev. B **39**, 13 086 (1989).
[61] J. Coste and J. Peyrard, Z. Phys. B **96**, 111 (1994).